EurJIC
European Journal of Inorganic Chemistry

Research Article
doi.org/10.1002/ejic.202200341

Chemistry Europe
European Chemical Societies Publishing

www.eurjic.org

Solvent-Dependent Self-Assembly of an Amphiphilic Copper(II) Complex with Bulky Head Groups

Constantin Schreck,[a] Johannes Weihermüller,[a] Peter Thoma,[a] Sabine Rosenfeldt,[b] Markus Drechsler,[c] Christoph Förster,[d] Katja Heinze,[d] Gerald Hörner,[a] and Birgit Weber*[a]

Dedicated to Prof. Wolfgang Beck on the occasion of his 90th birthday.

The aggregation behavior of an amphiphilic copper(II) complex was studied in solution by means of UV-Vis and EPR spectroscopy. While dilute solutions in polar media do not give indication of relevant intermolecular interactions, concentrated solutions in nonpolar media clearly do *not* reflect the molecular properties of **[CuL]** (H_2**L**: N_2O_2 ligand of the Jäger-type with bulky head-group and long alkoxy tailing). Massive broadening of EPR-lines is prevalent in non-polar media, such as *n*-heptane and *iso*-octane. In combination with DFT-modelling, the solvent-dependence of the EPR response (line widths and Cu-hyperfine coupling) could be associated with the formation of oligomers with weak anti-ferromagnetically coupled copper centers. Weak anti-ferromagnetic coupling becomes evident also by SQUID magnetometry at $T < 10$ K of solid samples of **[CuL]**. The tendency towards supramolecular aggregation is unequivocally shown by electron microscopy of dried (TEM) and frozen samples (cryo-TEM). While the former approach gives evidence of the formation of extended 2D sheet-like structures with extensions on the micrometer scale, the latter technique identifies the formation of 1D thread-like structures with lengths of several hundred nanometers.

Introduction

Assembly of molecular units into larger aggregates is a result of amplification of attractive interactions upon close encounters of the constituents. Biological structures broadly make full use of hydrogen bonds as the source of interaction and the structure-defining motif.[1] By contrast, utilization of dispersion forces as a weaker and undirected source of attraction gives necessarily more flexible structures. Self-assembly of amphiphilic molecules, for instance, may likewise yield (sub-)macroscopic structures, such as fibrils and sheets. Self-assembly of entirely organic amphiphils has been broadly studied. The formation of liquid crystals from amphiphils is probably the most striking example for emerging properties in aggregates.[2] By contrast, metalorganic systems are far less well known although they hold promise as a soft-matter access to tunable magnetic materials.[3]

Surfactants that are responsive to external magnetic fields are interesting for application due to their ready manipulation. Usually ionic liquids or surfactants are not responsive, because the isolated paramagnetic transition metal centers lack the necessary long-range interactions.[4] Controlled magnetic properties through self-assembly of (para-) magnetic amphiphilic molecules have been reported by Kurth and coworkers,[5] who equipped iron(II) with a rigid ditopic ligand to obtain a metallo-supramolecular coordination polyelectrolyte. The presence of dialkyl phosphoric acid esters brought about lipid-like behavior and liquid crystalline properties. Notably, the architecture (chain length) feeds back to the spin crossover properties of iron(II). A similar approach led Gütlich to the question: "Does the Solid-Liquid Crystal Phase Transition Provoke the Spin-State Change in Spin-Crossover Metallomesogens?"[6] More recently we have likewise studied the aggregation properties of amphiphilic iron(II) complexes and their feedback on magnetic behavior. Based on a systematic variation of molecular dimensions it was possible to analyze the packing in the crystal structures in terms of the ratio of two molecular rulers, that is, the size of the head group vs. the chain length of the alkyl residues.[7] Linear vs. tilted arrangement of the alkyl chains which prevails for iron(II) complexes allows prediction of lipid-layer like arrangements and its feedback on the magnetic properties in the context of spin crossover. Cooperativity of neighboring metal centers is evident from these studies,[8] but certainly is imposed by the

[a] C. Schreck, Dr. J. Weihermüller, Dr. P. Thoma, Dr. G. Hörner, Prof. Dr. B. Weber
Department of Chemistry, Inorganic Chemistry IV
University of Bayreuth
Universitätsstr. 30, 95440 Bayreuth, Germany
E-mail: weber@uni-bayreuth.de
[b] Dr. S. Rosenfeldt
Department of Chemistry, Physical Chemistry I
University of Bayreuth
Universitätsstr. 30, 95440 Bayreuth, Germany
[c] Dr. M. Drechsler
Keylab Electron and Optical Microscopy
Bavarian Polymer Institute
University of Bayreuth
Universitätsstr. 30, 95440 Bayreuth, Germany
[d] Dr. C. Förster, Prof. Dr. K. Heinze
Department of Chemistry
Johannes Gutenberg University Mainz
Duesbergweg 10–14, Mainz, Germany

Supporting information for this article is available on the WWW under https://doi.org/10.1002/ejic.202200341

Research Article
doi.org/10.1002/ejic.202200341

presence of bridging ligands.[7b] The question, whether amphiphilic complexes with open-shell metal ions will self-assemble to magnetic-responsive aggregates in the absence of a bridge motivates the present study. As a matter of fact, we have recently identified twisted nanowires as a result of aggregation of amphiphilic copper(II) complexes. Charge transport along the wires has been investigated, but the magnetic behavior was not studied.[9]

Here we report on the synthesis and characterization of an amphiphilic copper(II) complex. The presence of bulky phenyl substituents on the head groups was found to reflect in the spectroscopic properties as well as the aggregation behavior, which turns out to be strongly dependent on the solvent.

Results and Discussion

Synthesis and Characterization

The synthesis of the new ligand **H_2L** and its copper(II) complex **[CuL]** was performed analogously to procedures described previously (Scheme 1).[9,10] As a structural and spectroscopic reference, the analogous nickel(II) complex **[NiL]** was prepared. Elemental analysis of the ligand and the derived nickel and copper complexes match with solvent-free formulations. Accordingly, four-coordinate **[CuL]** is received; the possibility of partial expansion of the coordination sphere through supramolecular interactions will be discussed below.

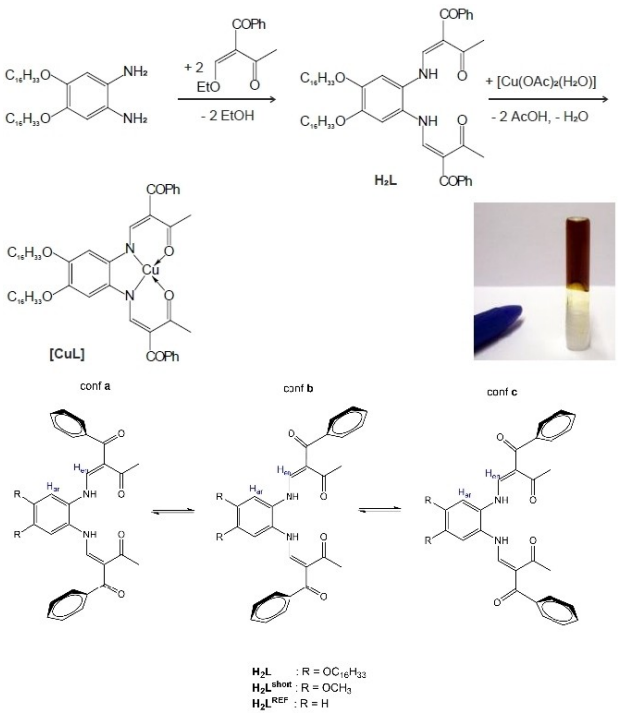

Scheme 1. (top) Synthesis and structure of the complex **[CuL]** and picture of the gel (2.3 wt% **[CuL]** in *iso*-octane); (bottom) rotamers of the ligands (in **$H_2L^{REF\text{-}ac}$** acetyl substitutes the benzoyl group (see below).

Concentrated solutions of **[CuL]** in nonpolar media are of a brownish appearance (see inset of Scheme 1). Spectra recorded of toluene solutions at very low concentration ($\ll 10^{-4}$ M; red in Figure 1A) relate the color impression to the vis-tailing of a broad and intense absorption band peaking at ca. 400 nm ($\varepsilon_{max} \approx 23{,}000\ M^{-1}cm^{-1}$). Significant absorption with $\varepsilon > 750\ M^{-1}cm^{-1}$ extends up to $\lambda = 450$ nm, while a broad band centered at $\lambda = 550$ nm is due to the copper(II) ligand-field transition ($\varepsilon_{max} \approx 500\ M^{-1}cm^{-1}$). Both of these features are absent in spectra of the ligand **H_2L** (black in Figure 1A). In agreement with the faint yellow color, vis absorption of the ligand in toluene is limited to the low-energy tailing of a strong band peaking at $\lambda = 360$ nm. The spectral response could be nicely matched with a TD-DFT-derived spectrum of the truncated model **[CuL^{short}]** (Figure 1B, conformer **a**). TD-DFT relates the diagnostic absorption band around 400 nm to an overlay of numerous individual transitions (verticals in Figure 1B). The leading components can be referred to intra-ligand charge-transfer from the alkoxy-substituted aryl to the chelate; some copper *d*-orbital contribution is noted, though. The spectral response is sensitive to both, the presence of the benzoyl moiety (see Ref. [10] for spectra of an acetyl derivative, **[CuL^{REF-ac}]**) and its conformation, predicting a slightly red-shifted near-UV envelope for conformer **b**.

The ^{1}H-NMR resonance pattern of the ligand **H_2L** (d_6-benzene and d_1-chloroform) largely reflects spectra previously recorded of similar N_2O_2 ligands with long alkoxy chains.[11] However, we note that the benzoyl moiety selectively affects the chemical shifts ascribable to the protons of phenylenediamine and the enamine C–H site. Both resonances are shifted to significantly higher field by $\Delta\delta > 0.15$ ppm, what indicates ring current like interactions with the π-system of the remote benzoylic group. Likewise, NMR spectra of the parent ligand **H_2L^{REF}** (R = H instead of $OC_{16}H_{33}$) give selective highfield shifts, which are absent in acetyl-substituted congeners. Due to massive line broadening, detailed discussion is not warranted of the NMR data of **[CuL]**. However, exchange for nickel(II) in **[NiL]**

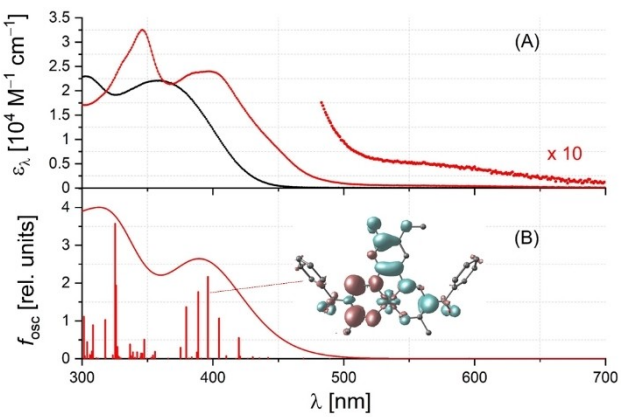

Figure 1. (A) UV-vis absorption spectra in toluene of **H_2L** (black) and **[CuL]** (red); (B) TD-DFT derived optical response of **[CuL^{short}]** (conformer **(a)**); verticals: individual transitions; solid line: convoluted and broadened spectrum; inset: TD-DFT-derived difference density of transition T18 ($\lambda = 389$ nm; $f_{osc} = 0.117$); source: green; sink: red.

Research Article
doi.org/10.1002/ejic.202200341

as a diamagnetic structure mimic for the paramagnetic copper(II) supports the notion of similar ring currents being active in the complexes as well.

As single crystals of **[CuL]** could not be obtained, the structure was modelled with DFT methods (for Computational Details, see the Experimental Section); calibration of structures and spectra with structurally known reference compounds (Tables S1–2, Supporting Information). Structure prediction reveals a distinct thermodynamic preference of conformers with close through-space contacts of the benzoyl π-system with the ligand backbone echoing conclusions from NMR; that is, conformer **a** of the ligand is slightly preferred over conformers **b** and **c** ([**a**]:[**b**]:[**c**]≈7.5:2.7:1.0; Scheme 1, bottom). In the copper(II) complex [$\mathbf{CuL}^{\mathbf{short}}$], conformers **a** and **b** are likewise close in energy, so that rapid turnover certainly occurs in solution. Accordingly, any spectral response will be weighted convolute of contributions of the individual components. The conformational preferences of the bulky benzoyl group must be expected to affect dispersion-governed supramolecular interactions and, thus, translate into the aggregation behavior.

Indications of Self-assembly in solution. Aggregation of copper complexes with benzoyl side chains [$\mathbf{CuL}^{\mathbf{REF}}$] had been suspected already by E.-G. Jäger in 1966;[12] Jäger deduced this from shifts in diagnostic vibrational markers and the energy of the ligand-field band. Aggregation phenomena must be expected to be even more prevalent in **[CuL]**, due to the presence of long alkoxy tails that support lipid-like interactions. Indeed, previous investigations of amphiphilic copper(II) complexes showed a very low solubility in most common solvents.[9] The introduction of the phenyl substituent in close proximity of the copper(II) center leads to a significantly increased solubility of the complex in toluene (up to 2.3 wt%), but also in *n*- and *iso*-octane, while the solubility in polar solvents remained very low. Interestingly, gel formation was observed for the *iso*-octane solutions within two days (Photograph in Scheme 1; less pronounced in *n*-octane and *n*-heptane). The gel showed thixotropy, thus shaking leads to a liquid again. In contrast to this, for the toluene solution no such behavior was observed. Obviously, self-assembly of **[CuL]** is solvent-dependent.

To probe the aggregation behavior of **[CuL]** in different solvents, X-band EPR spectra of **[CuL]** were recorded in toluene (2.0 wt%) and in *n*-heptane at concentrations of 0.2 and 2.0 wt%, respectively (Figure 2). Simulation of the spectra with different parameter sets gave fits of similar quality. Therefore, analogous to related salen copper(II) complexes,[13] the simulations consider an axial symmetry (g_1, $g_2=g_3$) of the spin system. Only the hyperfine coupling to copper ($^{63/65}$Cu, $I=3/2$, A_1, $A_2=A_3$) and an isotropic rotation in the molecular slow-motion regime, defined by the correlation time τ[14] are included to simulate the EPR spectral pattern. The unresolved hyperfine coupling to the ^{14}N nuclei ($I=1$) is taken into account by Voigtian line broadening in the simulation. Different aggregates, i.e. different EPR active Cu^{II} species, have not been taken into account. The EPR spectrum of **[CuL]** in toluene features a well-resolved broad quartet, due to the hyperfine interaction to the copper nucleus (Figure 2a). The correlation time was estimated to $\tau=10^{-9}$ s. Compared to typical values for

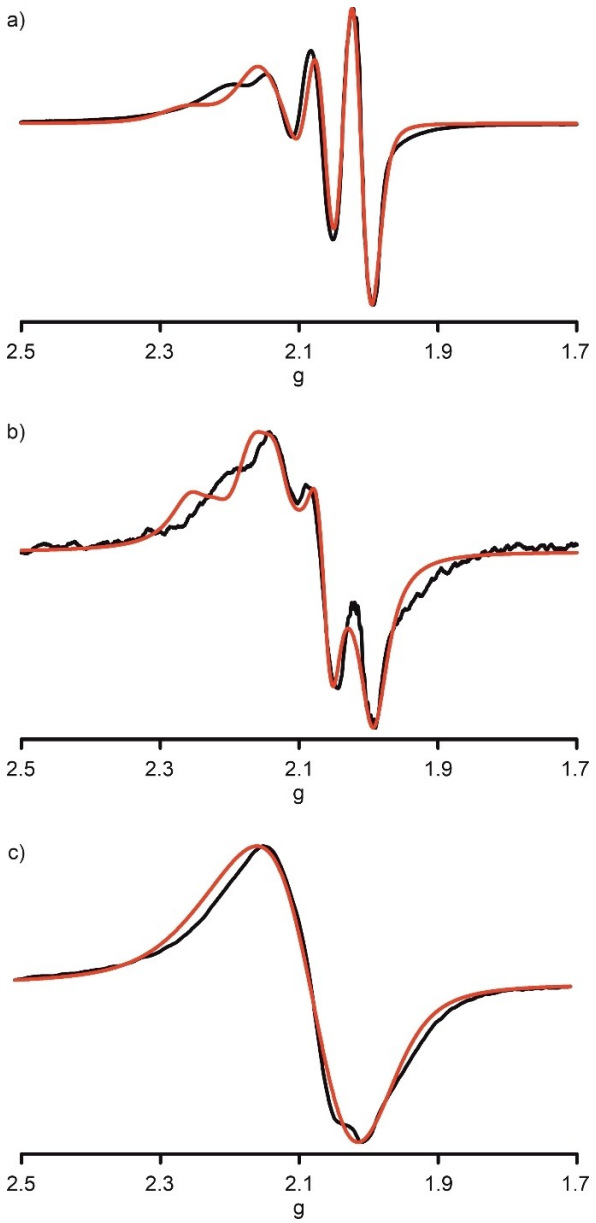

Figure 2. X-band EPR spectra (9.4 GHz) of **[CuL]**; a) in toluene (2.0 wt%, $g_1=2.137$, $g_2=g_3=2.062$; $A_1=437$ MHz, $A_2=A_3=128$ MHz, $\tau=10^{-9}$ s), b) in *n*-heptane (0.2 wt%, %, $g_1=2.117$, $g_2=g_3=2.072$; $A_1=370$ MHz, $A_2=A_3=107$ MHz, $\tau=10^{-5}$ s) and c) *n*-heptane (2 wt%, %, $g_1=2.105$, $g_2=g_3=2.068$; $A_1=281$ MHz, $A_2=A_3=51$ MHz, $\tau=10^{-3}$ s); black: experimental data; red: simulation.

copper(II) complexes ($\tau=30-100\times10^{-12}$ s for $M=250$–450 g mol^{-1}) in aqueous solution[15] this is very large, reflecting the high molecular mass of the monomer and probably indicating beginning aggregation. The spectrum of 0.2 wt% **[CuL]** in *n*-heptane is significantly more broadened (Figure 2b). The simulation yielded a much larger correlation time of $\tau=10^{-5}$ s. This is a consequence of formation of aggregates with high molecular mass. In addition, the copper hyperfine coupling constants decrease from $A_1=437$ MHz, $A_{2/3}=128$ MHz in toluene to $A_1=370$ MHz, $A_{2/3}=107$ MHz in *n*-heptane. This probably reflects interactions of the spin centers within the

Research Article
doi.org/10.1002/ejic.202200341

aggregates. Increasing the concentration to 2 wt% of **[CuL]** in *n*-heptane results in a single broad resonance without resolved fine structure (Figure 2c). A tentative interpretation of the simulation indicates a further increase of the degree of aggregation by raising the correlation time to $\tau = 10^{-3}$ s and by lowering the hyperfine coupling ($A_1 = 281$ MHz, $A_{2/3} = 51$ MHz). Interestingly, DFT likewise identifies hyperfine coupling in dimers to be much weaker than in mononuclear species (Table S3, SI).

Solvent-dependent self-assembly of **[CuL]** is supported further by a comparison of the small-angle X-ray scattering data in *iso*-octane, *n*-octane and toluene, shown in Figure 3A. A significant signal was only obtained for the octane solutions, hinting to molecularly dissolved **[CuL]** in toluene and to self-assembly in *iso*- and *n*-octane. The different slopes at intermediate *q*-values indicate a higher spatial dimension of the self-assembled structure in *iso*-octane. SAXS data of a dried **[CuL]** gel on mica (Figure 3B, starting solution was 1.2 wt% **[CuL]** in *iso*-octane) shows both pronounced and weaker Debye-Scherer rings, which confirms that **[CuL]** self-assemblies from *iso*-octane have a high degree of order. The intense rings roughly correspond to dimensions of 4.1 nm, 2.0–1.9 nm and 1.4 nm and the less intense ones to approximately 1.1 nm and 0.4 nm.

Plausible aggregation modes of **[CuL]** were assessed through DFT methods. For sake of computational costs, dimers of the truncated model, $[\mathbf{CuL^{short}}]_2$, have been optimized starting from three reasonable structures (plots of the optimized structures in Figure S8, Supporting Information). The starting structures reflect (i) the known preference of related complexes to form dispersion-dimers via π-stacks with minor axial interactions at copper[10] or (ii) the axial expansion of the coordination sphere to CN = 4 + δ through bonding interaction with the remote carbonyls. The latter mode has been recently suggested for the self-association of zinc complexes in planar N_2O_2 fields.[16] While this fragmentary scan of the conformational space cannot be expected to be fully conclusive, some relevant conclusions can be drawn. In the previously reported zinc(II)-based dimers strong axial interactions have overridden van der Waals interactions. Clearly, copper is much less prone to such axial ligation than zinc. An overall energy difference of *ca.* 20 kJ mol^{-1} is in favor of the dispersion dimers. This preference largely reflects the enhanced van der Waals attractions of the co-parallel π-planes of the complex units (dihedral < 2.5°) held at a distance of ca. 3.1 Å (non-bonded Cu···Cu distance 4.99 Å), but also integrates the beneficial interactions among adjacent benzoyl π-planes (see Figure 4). Similar favorable global π-interactions are not available in the other optimized structures.

As shown by broken-symmetry calculations, the copper centers in the computed dimers are not independent of each other. For the dimer of lowest energy, we identify very weak anti-ferromagnetic coupling between adjacent copper centers ($J = -0.5$ cm^{-1}). This coupling is expected to govern the magnetic behavior at low temperature.

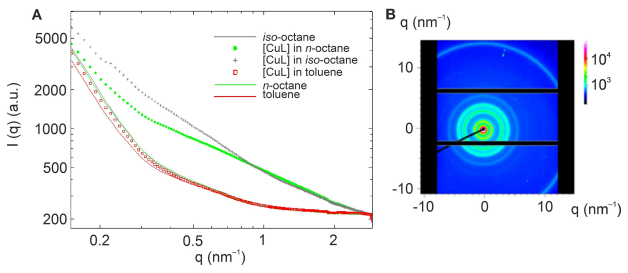

Figure 3. A. Small-angle X-ray scattering (SAXS) data of solvent-dependent self-assembly of **[CuL]** (beamline P03 at Petra III/DESY; concentration of **[CuL]**: 1.2 wt% in *iso*-octane, 1.5 wt% in *n*-octane and saturation concentration in toluene). The samples were gels in both octanes and liquid-like in toluene. B. SAXS data of dried [CuL] gel on mica.

Magnetic properties

The magnetic properties of **[CuL]** were investigated both in solution and in the solid state. Magnetic susceptibility measurements of the bulk complex were performed between 2 K and 250 K using a SQUID magnetometer; application of different magnetic fields did not affect the results (2,000 Oe and 20,000 Oe). The results are shown in Figure 5 as plot of the effective Bohr magneton number (μ_{eff}) vs. the temperature. The plots show three different domains: The starting value at $T =$ 250 K of $\mu_{eff} \approx 2.4$ is compatible with an $S = {}^1/_2$ spin system with quite substantial contributions from orbital momentum; while

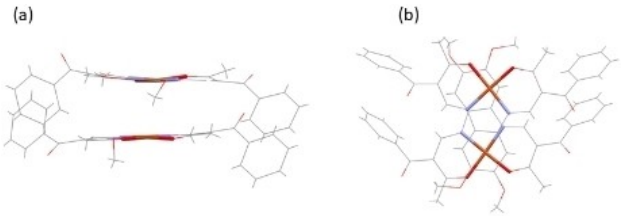

Figure 4. Optimized structure of the π-dispersion dimer (180°)) of the truncated model $[\mathbf{CuL^{short}}]_2$; a) side-view of the stacked coordination sites (dihedral 2.5°), b) top view of the head-to-tail arrangement (*d*(Cu···Cu) = 4.99 Å).

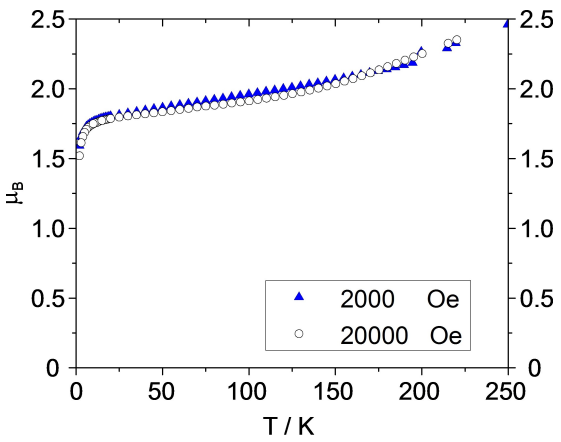

Figure 5. SQUID-Measurements of **[CuL]** in the temperature range between 2 K and 250 K at two different external magnetic fields.

Research Article
doi.org/10.1002/ejic.202200341

this value is certainly large, it is still not uncommon for copper(II) complexes. Starting from $T = 250$ K, the effective magnetic moment tends to decrease continuously with the temperature, running into an almost constant plateau value of $\mu_{eff} = 1.83$ between $10\ K < T < 70\ K$. The latter value is close to the expected spin-only value of 1.73 for an $S = {}^1/_2$ spin system and indicates that there is little orbital angular momentum left in this temperature range. Temperature-dependent quenching and restoration of orbital magnetic moments has been identified recently in mononuclear cobalt(II) systems.[17] In the cited study, the temperature dependence has been associated with dynamic (de-)coordination of an additional donor atom. A similarly satisfying interpretation of the dynamics in **[CuL]** is not at hands. Upon cooling below 10 K the magnetic moment decreases abruptly. Such a decrease is often an indication of very weak antiferromagnetic interactions, due to short contacts in the solid. We note, that treatment of the aforementioned dispersion dimers $[\mathbf{CuL}^{\mathbf{short}}]_2$ with a broken-symmetry approach indeed supports our notion of weak antiferromagnetic coupling between the non-bonded copper atoms (d(Cu···Cu) = 3.18 Å and 4.99 Å, for mutual rotation of the modules by 90° and 180°, respectively). Fits to the Bleaney-Bowers coupling model[18] yielded unexceptional values for the temperature independent magnetism TIP and the Landé factor g (Figure S9 and Table S4). The coupling constants $J = -1.01\ cm^{-1}$ and $J = -1.24\ cm^{-1}$, however, nicely match the DFT results.

The response of droplets of a **[CuL]** solution in *iso*-octane and toluene to a magnetic field was investigated. Representative images of the drops are given in the SI (Figure S10). The drop profiles in presence and absence of an external magnetic field are almost identical in both cases and thus give no indication for magnetic responsiveness.

Aggregates in Transmission Electron Microscopy (TEM)

TEM and cryo-TEM images of the dried or frozen solutions of **[CuL]** in *iso*-octane were recorded at different complex concentrations, see Figure 6 (TEM) and Figure 7 (cryo-TEM). The contrast between the copper-containing head-group and the alkyl chains allows depiction of the aggregates shape. Due to the higher electron density, the copper containing parts are expected to appear darker than the alkyl parts. The TEM images in Figure 6 reveal that, upon drying, thin films are obtained with no obvious superstructures or lipid layer-like arrangements.

The films roll or fold up indicating high flexibility, but no further structural information can be obtained. By contrast, the cryo-TEM images given in Figure 7 identify very thin but long fibers. For the more concentrated solutions (Figure 7A–D), a parallel alignment of the fibers is observed leading to layer like structures. Due to the close packing the single fibers are difficult so see. This alignment could be an explanation for the thin films observed in the TEM images, formed upon drying. More dilute solutions were used for the cryo-TEM images shown in Figure 7E and Figure 7F. Here, the single fibers are better isolated and more clearly visible. As the fibers appear darker than their

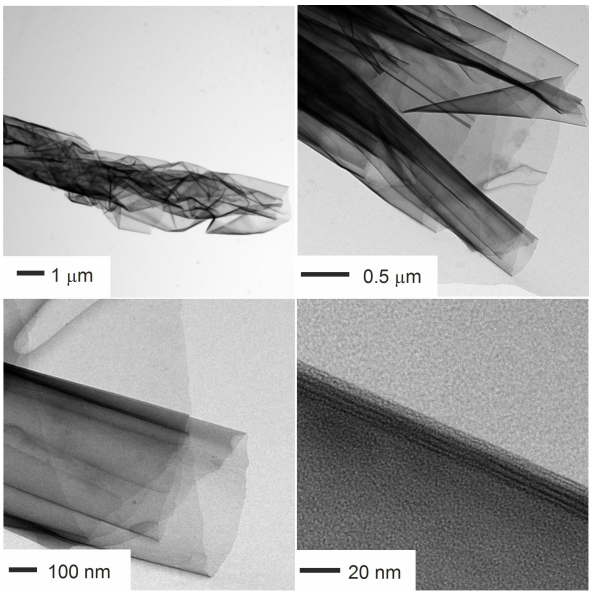

Figure 6. TEM images of a dried solution of **[CuL]** in *iso*-octane (2.3 wt%) at different magnifications.

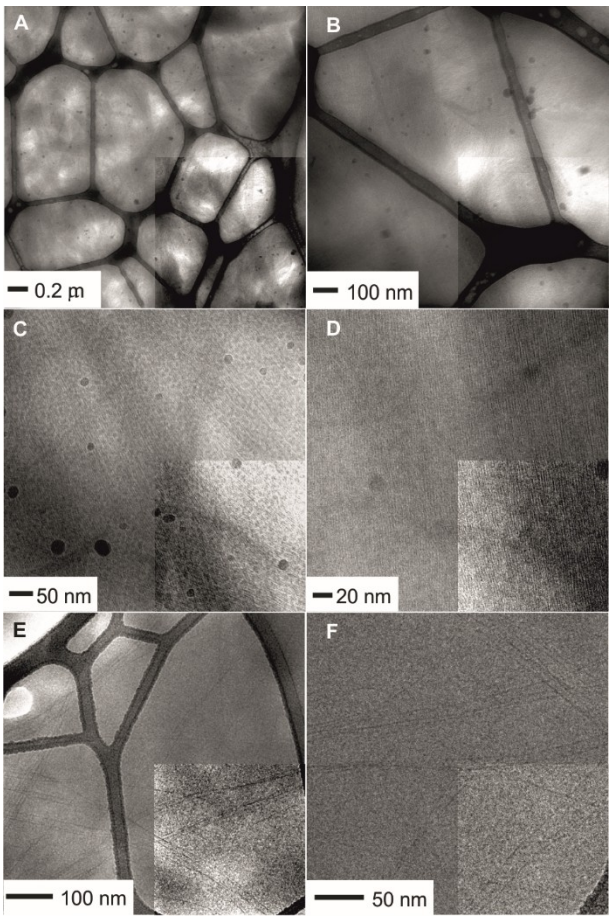

Figure 7. Cryo-TEM images of a frozen solution of 1.2 wt% **[CuL]** in *iso*-octane (A–D) and 0.12 wt% **[CuL]** in *iso*-octane (E,F) at different magnifications. To highlight the fibres, the bottom right section of each image is displayed with increased contrast.

Research Article
doi.org/10.1002/ejic.202200341

surrounding, they are most likely formed by the copper-containing head groups of the amphiphilic molecules, whereas the alkyl chains should have a similar contrast as the solvent *iso*-octane and are thus not visible.

An obvious explanation for the formation of fibers in alkanes and their absence in toluene is the different solubility of both, the head group and the tail in the two solvents. Apparently, in toluene the solubility of both parts of the amphiphilic molecule is similar leading to isolated molecules with no significant intermolecular interactions. By contrast, the alkanes will be much more selective media for the alkyl chains. The columnar structure thus suggests stacked Schiff base-like ligand parts with the alkyl chains pointing outwards, as illustrated schematically in Scheme 2. Such structures will be stabilized further by intermolecular interactions between the head-groups. Single crystal X-ray structures of copper(II) complexes of related ligands without alkyl chains and the DFT calculations support these considerations. The almost planar complexes show stacking arrangements stabilized by π-π- or metal-π-interactions.[10]

Conclusions

The way how intermolecular interactions among molecular constituents translate into macromolecular structure and function is largely unknown in many cases, notwithstanding the central importance of this question for disciplines like structural biology and material science (to name only two examples). In our present study on the aggregation behavior of an amphiphilic copper(II) complex, we made some observations which may prove relevant to these questions. As shown by electron microscopy of authentic frozen solutions of **[CuL]** in nonpolar media (cryo-TEM), supramolecular interactions culminate in the formation of well-defined fibril-like structures. Whereas EPR spectra of these solid samples were not available, spectra of concentrated solutions of the complex **[CuL]** are clearly not attributable to molecularly dissolved species, even at room temperature. Aggregation is thereby found to be strongly solvent dependent, as EPR line-widths tended to increase strongly with a decrease of solvent polarity. These observations echo our expectations in that the $[CuN_2O_2]$ coordination sites will be increasingly shielded from solution, leading to close Cu···Cu contacts in the aggregates. Accordingly, such contacts are electronically relevant as they shine up both in solid samples (SQUID magnetometry) and in solution (EPR spectroscopy) and can be traced by DFT modelling also in binuclear models of the aggregates. Intriguingly, however, the shape of the aggregates formed is somewhat at odds with our expectations. Previous work of our lab had shown that similar copper(II) complexes arrange into twisted helical structures. By contrast, the present work gave no indication of twisted structures. This difference points to a major steering role of the substitution pattern of the N_2O_2 chelate moieties on the nature and quality of the supramolecular interactions.

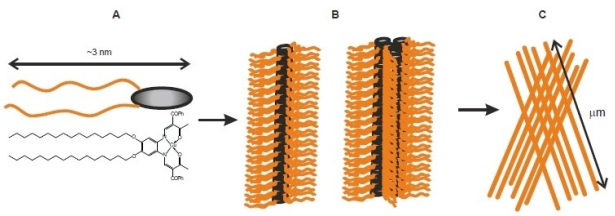

Scheme 2. (top) Illustration of the potential stacking motives of the amphiphilic complex **[CuL]** with an almost planar head group leading to long fibers.

Experimental Section

All reagents were of reagent grade and used without further purification. All solvents were of analytical grade and used without further purification. The synthesis of 1,2-diamino-4,5-dihexadecyloxybenzene[8] and the keto-enol-ether[12] was described previously. The syntheses of the ligands $\mathbf{H_2L}$ and $\mathbf{H_2L^{Ref}}$ as well as of the complex $\mathbf{[CuL^{Ref}]}$ were performed analogously to procedures described previously.[12]

Synthesis of $\mathbf{H_2L}$.5.0 g (8.4 mmol) 1,2-diamino-4,5-dihexadecyloxy-benzen and 4.07 g (18.67 mmol) of the keto-enol-ether were mixed in 250 mL ethanol and heated to reflux for 1.5 h. After cooling to −28 °C overnight the formed precipitate was separated by filtration, washed two times with 10 mL ice-cold ethanol and dried under vacuum. Yield: 7.29 g (7.81 mmol, 92 %). $C_{60}H_{88}N_2O_6$ (933.37 g mol^{-1}); calcd. C 77.21; H 9.50; N 3.00; found: C 77.07; H 9.26; N 2.86. **FT-IR** [cm^{-1}]: $\tilde{\nu}$ = 2914 (s, [–C–H]), 2848 (s, [–C–H]), 1619 (s, [C=C]), 1266 (s, [C–N]), 1198 (s, [C–O]), 721 (m, [C–H]).

^{1}H NMR (300 MHz, C_6D_6, 25 °C): δ = 12.95 (d, *J* = 12.3 Hz, 2 H, N*H*), 7.78–7.71 (m, 4 H, C(O)–C_{Ar}–C_{Ar}*H*), 7.58 (d, *J* = 12.2 Hz, 2 H, NH–C*H*), 7.15–7.06 (m, 6 H, C(O)–C_{Ar}–C_{Ar}H–C_{Ar}*H*–C_{Ar}*H*), 6.22 (s, 2 H, NH–C_{Ar}–C_{Ar}*H*), 3.53 (t, *J* = 6.3 Hz, 4 H, O–C*H*$_2$), 2.61 (s, 6 H, C(O)–C*H*$_3$), 1.70–1.58 (m, 4 H, O–CH$_2$–C*H*$_2$), 1.48–1.25 (m, 52 H, CH$_2$–C*H*$_2$–CH$_{2/3}$), 0.95–0.89 (m, 6 H, CH$_2$–C*H*$_3$).

^{1}H NMR (300 MHz, $CDCl_3$, 25 °C): δ = 12.67 (d, *J* = 12.3 Hz, 2 H, N*H*), 7.72–7.63 (m, 6 H, C(O)–C_{Ar}–C_{Ar}*H*; NH–C*H*), 7.55–7.39 (m, 6 H, C(O)–C_{Ar}–C_{Ar}H–C_{Ar}*H*–C_{Ar}*H*), 6.51 (s, 2 H, NH–C_{Ar}–C_{Ar}*H*), 3.86 (t, *J* = 6.6 Hz, 4 H, O–C*H*$_2$), 2.51 (s, 6 H, C(O)–C*H*$_3$), 1.81–1.68 (m, 4 H, O–CH$_2$–C*H*$_2$), 1.48–1.25 (m, 52 H, CH$_2$–C*H*$_2$–CH$_{2/3}$), 0.91–0.83 (m, 6 H, CH$_2$–C*H*$_3$).

Synthesis of **[CuL]**: 1.68 g (1.8 mmol) $\mathbf{H_2L}$ and 0.36 g (1.8 mmol) copper(II)acetate monohydrate were heated to reflux in 250 mL ethanol for 2 h. After cooling to room temperature, the brownish precipitate was separated by filtration, washed two times with 10 mL ethanol and dried under vacuum. Yield: 1.44 g (1.44 mmol, 89 %). $C_{60}H_{86}CuN_2O_6$ (994.90 g mol^{-1}); calcd. C 72.44; H 8.71; N 2.82; found: C 72.43; H 8.63; N 2.74. **FT-IR** [cm^{-1}]: $\tilde{\nu}$ = 2916 (s, [–C–H]), 2849 (s, [–C–H]), 1570 (s, [C=C]), 1280 (s, [C–N]) 720 (m, [C–H]).

Synthesis of **[NiL]**: 0.20 g (0.21 mmol) $\mathbf{H_2L}$ and 0.06 g (0.25 mmol) nickel(II)acetate tetrahydrate were heated to reflux in 30 mL ethanol for 3 h. After cooling to −23 °C overnight an orange precipitate formed, which was separated by filtration, washed two times with 10 mL ice-cold ethanol and dried under vacuum. Yield: 0.19 g (0.19 mmol, 88 %). $C_{60}H_{86}N_2NiO_6$ (990.05 g mol^{-1}); calcd. C 72.79; H 8.76; N 2.83; found: C 73.08; H 8.45; N 2.76. **FT-IR** [cm^{-1}]: $\tilde{\nu}$ = 2915 (s, [–C–H]), 2848 (s, [–C–H]), 1569 (s, [C=C]), 1282 (s, [C–N]) 720 (m, [C–H]).

^{1}H NMR (500 MHz, C_6D_6, 25 °C) δ = 7.88 (s, 2 H, N–C*H*), 7.71–7.64 (m, 4 H, C(O)–C_{Ar}–C_{Ar}*H*), 7.14–7.05 (m, 6 H, C(O)–C_{Ar}–C_{Ar}H–C_{Ar}*H*–C_{Ar}*H*),

6.60 (s, 2 H, N–C_{Ar}–$C_{Ar}H$), 3.52 (t, J = 6.3 Hz, 4 H, O–CH_2), 2.34 (s, 6 H, C(O)–CH_3), 1.72–1.56 (m, 4 H, O–CH_2–CH_2), 1.49–1.20 (m, 52 H, CH_2–CH_2–$CH_{2/3}$), 0.93 (t, J = 6.7 Hz, 6 H, CH_2–CH_3).

^{1}H NMR (500 MHz, $CDCl_3$, 25 °C) δ = 7.74 (s, 2 H, N–C*H*), 7.72–7.65 (m, 4 H, C(O)–C_{Ar}–$C_{Ar}H$), 7.56–7.39 (m, 6 H, C(O)–C_{Ar}–C_{Ar}H–$C_{Ar}H$–$C_{Ar}H$), 6.66 (s, 2 H, N–C_{Ar}–$C_{Ar}H$), 3.81 (t, J = 6.7 Hz, 4 H, O–CH_2), 2.33 (s, 6 H, C(O)–CH_3), 1.77–1.68 (m, 4 H, O–CH_2–CH_2), 1.48–1.25 (m, 52 H, CH_2–CH_2–$CH_{2/3}$), 0.88 (t, J = 6.9 Hz, 6 H, CH_2–CH_3).

For **elemental analysis**, the carbon, nitrogen, and hydrogen contents were determined with a Unicube (Elementar Analysensysteme GmbH) with sulfanilamide as standard. The samples were placed in tin boats and measured at least twice.

^{1}H NMR spectroscopic measurements were done on a Bruker Avance 300 MHz spectrometer or on a Bruker Avance III HD 500 MHz spectrometer at 25 °C.

FT-IR spectra were recorded at 25 °C using a Bruker IFS66v spectrometer in the range of 400–4000 cm^{-1}.

X-band EPR spectra were recorded on a Miniscope MS 300 (Magnettech GmbH, Germany) with a frequency counter from Hewlett-Packard at a microwave frequency of 9.42 GHz (295 K). Mn^{2+} in ZnS was used as the external standard (g = 2.118, 2.066, 2.027, 1.986, 1.946, 1.906). Simulations were performed with the program package Easyspin for MatLab (R2016b).[19]

Magnetic susceptibility measurements were performed using a Quantum Design MPMS-XL-5 SQUID magnetometer. A field strength of 0.2 and 2.0 T was applied and a temperature range of 5–250 K was used to determine the temperature dependency of the magnetism. The measurements were performed in settle mode with an average cooling and heating rate of 0.5 K min^{-1}. The samples were prepared in gelatine capsules placed in a plastic straw. The measured values were corrected for the diamagnetism of the sample holder and the ligand (tabulated Pascal constants).[20]

Transmission electron microscopy (TEM) was taken at a JEOL JEM-2200FS electron microscope. The solution was dropped on a carbon coated copper grid (mesh 200, Science Services, Munich). Electron acceleration voltage was set to 200 kV. Micrographs were taken with an OneView 1095 / DigitalMicrograph GMS 3.2 system from Gatan (Munich, Germany). The microscope is an Energy-Filtering TEM (EFTEM). All micrographs were acquired in near focus bright field mode and zero-loss filtered. An objective aperture of 120 μm was used.

For cryo-TEM studies, a sample droplet of 2 μL was put on a lacey carbon filmed copper grid (Science Services, Munich, Germany). Subsequently, most of the liquid was removed with blotting paper leaving a thin film stretched over the lace holes. The specimens were instantly shock frozen by rapid immersion into liquid nitrogen in a temperature-controlled freezing unit (Zeiss Cryobox, Carl Zeiss Microscopy GmbH, Jena, Germany). The temperature was monitored and kept constant in the chamber during all the sample preparation steps. The specimen was inserted into a cryotransfer holder (CT3500, Gatan, Munich, Germany) and transferred to a Zeiss / LEO EM922 Omega EFTEM (Zeiss Microscopy GmbH, Jena, Germany). Examinations were carried out at temperatures around 90 K. The TEM was operated at an acceleration voltage of 200 kV. Zero-loss filtered images (ΔE = 0 eV) were taken under reduced dose conditions (100—1000 e nm^{-2}). All images were registered digitally by a bottom mounted CCD camera system (Ultrascan 1000, Gatan, Munich, Germany) combined and processed with a digital imaging processing system (Digital Micrograph GMS 1.9, Gatan, Munich, Germany).

Computational Details. Electronic structure calculations on the complexes have been performed through density-functional theory (DFT) methods using the ORCA program package.[21] In all optimizations triple-ξ-valence TZVP basis sets[22] were used with the generalized gradient approximated functional BP86.[23] The optimized ligand and the complexes were verified as stationary points through the absence of imaginary modes in numerical frequency calculations. Cartesian Coordinates of the optimized structures are given in Tables S5–17 in the Supporting Information. Electronic properties were extracted from single-point calculations in the optimized positions with B3LYP (EPR)[24] and the global hybrid functional TPSSh (UV-vis; broken symmetry)[25] using triple-ξ-valence TZVP basis sets. Grimme's third generation D3 correction of dispersion was used,[26] medium effects were approximated in a dielectric continuum approach (COSMO), parameterised for chloroform.[27] For the complex **[CuL^{short}]** the 80 lowest optical electronic transitions were assessed with ORCA implemented TD-DFT methods within the Tamm-Dancoff approximation.

Acknowledgements

G.H. and B.W. acknowledge financial support of Deutsche Forschungsgemeinschaft (Project 463161096). The authors thanks DESY(Hamburg, Germany), a member of the Helmholtz Association HGF, the staff of beamline P03, especially Dr. Stephan V. Roth, for providing time for the test measurements. Open Access funding enabled and organized by Projekt DEAL.

Conflict of Interest

The authors declare no conflict of interest.

Data Availability Statement

The data that support the findings of this study are available from the corresponding author upon reasonable request.

Keywords: Aggregation · Amphiphilic complexes · Copper · Magnetism · Self-assembly

[1] G. R. Desiraju, T. Steiner in *The weak hydrogen bond. In structural chemistry and biology, International Union of Crystallography monographs on crystallography, Vol. 9*; (Eds. G. R. Desiraju, T. Steiner), Oxford University Press, Oxford, **2001**, pp. 343–440.
[2] D. Andrienko, *J. Mol. Liq.* **2018**, *267*, 520–541.
[3] D. R. Talham, *Chem. Rev.* **2004**, *104*, 5479–5502.
[4] P. Brown, A. Bushmelev, C. P. Butts, J. Cheng, J. Eastoe, I. Grillo, R. K. Heenan, A. M. Schmidt, *Angew. Chem. Int. Ed.* **2012**, *51*, 2414–2416; *Angew. Chem.* **2012**, *124*, 2464–2466.
[5] a) Y. Bodenthin, U. Pietsch, H. Möhwald, D. G. Kurth, *J. Am. Chem. Soc.* **2005**, *127*, 3110–3114; b) Y. Bodenthin, G. Schwarz, Z. Tomkowicz, T. Geue, W. Haase, U. Pietsch, D. G. Kurth, *J. Am. Chem. Soc.* **2009**, *131*, 2934–2941; c) Y. Bodenthin, G. Schwarz, Z. Tomkowicz, M. Lommel, T. Geue, W. Haase, H. Möhwald, U. Pietsch, D. G. Kurth, *Coord. Chem. Rev.* **2009**, *253*, 2414–2422.
[6] a) A. B. Gaspar, M. Seredyuk, P. Gütlich, *Coord. Chem. Rev.* **2009**, *253*, 2399–2413; b) M. Seredyuk, A. B. Gaspar, V. Ksenofontov, Y. Galyametdinov, J. Kusz, P. Gütlich, *J. Am. Chem. Soc.* **2008**, *130*, 1431–1439.

[7] a) S. Schlamp, P. Thoma, B. Weber, *Chem. Eur. J.* **2014**, *20*, 6462–6473; b) J. Weihermüller, S. Schlamp, W. Milius, F. Puchtler, J. Breu, P. Ramming, S. Hüttner, S. Agarwal, C. Göbel, M. Hund, G. Papastavrou, B. Weber, *J. Mater. Chem. C* **2019**, *7*, 1151–1163; c) J. Weihermüller, S. Schlamp, B. Dittrich, B. Weber, *Inorg. Chem.* **2019**, *58*, 1278–1289.
[8] S. Schlamp, B. Weber, A. D. Naik, Y. Garcia, *Chem. Commun.* **2011**, *47*, 7152–7154.
[9] C. Isenberg, E. B. Käkel, T. P. I. Saragi, P. Thoma, B. Weber, A. Lorenz, *RSC Adv.* **2019**, *9*, 1807–1813.
[10] C. Lochenie, S. Schlamp, A. P. Railliet, K. Robeyns, B. Weber, Y. Garcia, *CrystEngComm* **2014**, *16*, 6213.
[11] S. Schlamp, P. Thoma, B. Weber, *Eur. J. Inorg. Chem.* **2012**, *2012*, 2759–2768.
[12] L. Wolf, E.-G. Jäger, *Z. Anorg. Allg. Chem.* **1966**, *346*, 76–91.
[13] a) H. Kanso, R. M. Clarke, A. Kochem, H. Arora, C. Philouze, O. Jarjayes, T. Storr, F. Thomas, *Inorg. Chem.* **2020**, *59*, 5133–5148; b) G. Verquin, G. Fontaine, E. Abi-Aad, E. Zhilinskaya, A. Aboukaïs, J.-L. Bernier, *J. Photochem. Photobiol. B* **2007**, *86*, 272–278.
[14] M. S. Bukharov, V. G. Shtyrlin, G. V. Mamin, A. S. Mukhtarov, E. M. Gilyazetdinov, *J. Phys. Conf. Ser.* **2012**, *394*, 12030.
[15] J. S. Hyde, W. Froncisz, *Ann. Rev. Biophys. Bioeng.* **1982**, *11*, 391–417.
[16] H. Kurz, G. Hörner, O. Weser, G. Li Manni, B. Weber, *Chem. Eur. J.* **2021**, *27*, 15158–15170.
[17] S.-Q. Su, S.-Q. Wu, M. L. Baker, P. Bencok, N. Azuma, Y. Miyazaki, M. Nakano, S. Kang, Y. Shiota, K. Yoshizawa, S. Kanegawa, O. Sato, *J. Am. Chem. Soc.* **2020**, *142*, 11434–11441.
[18] B. Bleaney, K. D. Bowers, *Proc. R. Soc. London Ser. A* **1952**, *214*, 451–465.
[19] S. Stoll, A. Schweiger, *J. Magn. Reson.* **2006**, *178*, 42–55.
[20] O. Kahn, *Molecular Magnetism*, VCH, New York, N.Y, **1993**.
[21] F. Neese, *WIREs Comput. Mol. Sci.* **2012**, *2*, 73–78.
[22] A. Schäfer, H. Horn, R. Ahlrichs, *J. Chem. Phys.* **1992**, *97*, 2571–2577.
[23] Becke, *Phys. Rev. A* **1988**, *38*, 3098–3100.
[24] A. D. Becke, *J. Chem. Phys.* **1993**, *98*, 5648–5652.
[25] V. N. Staroverov, G. E. Scuseria, J. Tao, J. P. Perdew, *J. Chem. Phys.* **2003**, *119*, 12129–12137.
[26] a) S. Grimme, J. Antony, S. Ehrlich, H. Krieg, *J. Chem. Phys.* **2010**, *132*, 154104; b) S. Grimme, S. Ehrlich, L. Goerigk, *J. Comput. Chem.* **2011**, *32*, 1456–1465.
[27] A. Klamt, G. Schüürmann, *J. Chem. Soc. Perkin Trans. 2* **1993**, 799–805.

Manuscript received: May 27, 2022
Revised manuscript received: July 26, 2022
Accepted manuscript online: July 28, 2022